Bubbly Flows through a Convergent–Divergent Nozzle

by

Hiroo YONECHI*, Maki SUZUKI**, Ryuji ISHII** and Shigeki MORIOKA**

(Received December 11, 1991)

Abstract

Characteristics of bubbly flow with a small void fraction through a vertical, two-dimensional, converging–diverging nozzle are investigated experimentally and numerically. Emphasis is placed on the mechanism for large velocity slip near the nozzle throat, where the pressure gradient is very large. Bubble velocities are measured by taking double-exposure photographs with stroboscopic light sources having a flash duration of a few μ sec. The pressure distribution of the mixture along the nozzle axis is measured by semiconductor pressure transducers. The local liquid velocity is determined through continuity equations of gas and liquid in conjunction with the measured data of pressure distribution and experimental conditions at the nozzle inlet and exit. The power spectrum density of the pressure fluctuations is measured to investigate some instabilty of the bubbly flow, which is believed to be inherent to the velocity slip. It is proved that the numerical results using Wijngaarden's model equations agree well with the experiments. The characteristics of flow instability are explained according to the theoretical predictions of Morioka et al.

1. Introduction

A mixture composed of liquid and dispersed gas bubbles exists in various kinds of engineering facility such as liquid metal MHD generator, boiling heat transfer system of nuclear power plant, sewage treatment, reactors in chemical industries and so on. In the designing and maintenance of these facilities sufficient knowledge of flow characteristics of the bubbly flow is crucially important to keep sound security. So far, many experimental and theoretical studies have been reported, and various important characteristics of the bubbly flow have been made clear[1-6]. In spite of this, however, there yet remain some curious or strange phenomena in the bubbly flow which will be physically interesting and important but cannot always be explained well physically and theoretically[5].

* Mitsubishi Electric Corporation, Kamakura
** Department of Aeronautical Engineering, Kyoto University

In general the bubbly flow is very complicated because bubbles change their shape and volume along their streamlines in the flow and also interact directly with each other, in some cases to coalesce or to break up. At least for the present, therefore, the construction of general and reasonable model equations for the bubbly flows has not succeeded. Only for dilute suspensions (with small void fraction), we can get a closed system of basic equations without serious difficulties[7,8].

In the present paper, first we consider the steady, subsonic-like flow of gas-liquid mixtures with a small void fraction in a converging-diverging nozzle. Our main attention is paid to the investigation of velocity slip near the nozzle throat. The experiments are performed in a water-nitrogen blowdown facility. The pressure at the reservoir is always kept at an atmospheric pressure and then the controlling parameters are the pressure at the nuzzle exit and the volume flow rate of the gas to that of the liquid. The effect of gravitational force cannot be neglected here and then the scale of the facility affects the flow.

Bubble velocities are measured on photographs which are taken by two successive exposures at a suitable time interval using stroboscopic light sources having a flash duration of a few μ sec. The pressure distribution of the mixture along the nozzle axis is measured at four locations along the nozzle axis : upstream of the throat, at the throat and downstream of the throat, by using pressure transducers. The liquid velocity is determined through continuity equations of gas and liquid with the measured data of pressure distribution of the mixture along the nozzle axis in conjunction with the flow conditions at the nozzle inlet and the exit. For investigation of the unstable phenomena inherent to the velocity slip, the power spectrum density of the pressure fluctuation is also measured.

In order to explain the experimental results, Wijngaaden's model equations are solved numerically for the same nozzle geometry and flow conditions as those in the experiments. A time-dependent method with the two-step MacCormack scheme is used for the numerical simulation. At first, a steady flow solution is obtained for the specified conditions at the nozzle inlet and exit. Next, pressure fluctuations are artificially imposed at the nozzle inlet to simulate the development of fluctuations in the nozzle.

Experimental and numerical results are compared with each other to discuss the physical mechanisms for the occurrence of large velocity slip, generation of unstable waves due to the velocity slip and cutoff of propagation waves with high frequency.

2. Experiments

2-1. Experimental apparatus

A schematic diagram of the water-nitrogen two-phase blowdown facility is shown in Fig. 1. This is essentially the same as that reported in Ref. 5 and consists of three main parts : the upstream tank, the test section, and the downstream dump tank. The upstream

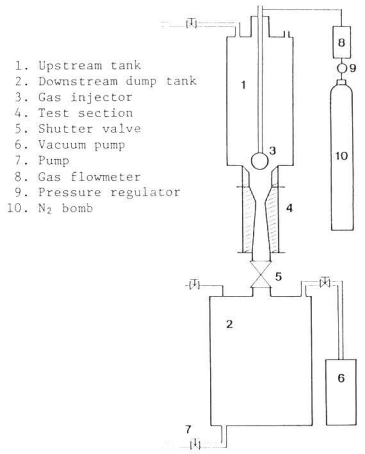

Fig. 1 Schematic diagram of water–nitrogen blowdown facility.

tank and the test section are made of transparent acrylic resin. The details of the test section and its photograph are shown in Figs. 2 and 3, respectively.

First, some amount of water is put into the upstream tank which has a constant cross-sectional area. The downstream tank is depressurized to a specified value by a vacuum pump. Then the shutter valve mounted between the nozzle exit and the downstream tank is opened. The water in the upstream tank and the gas from the injector are mixed and are blown down through the test section to the downstream tank. The running time for each

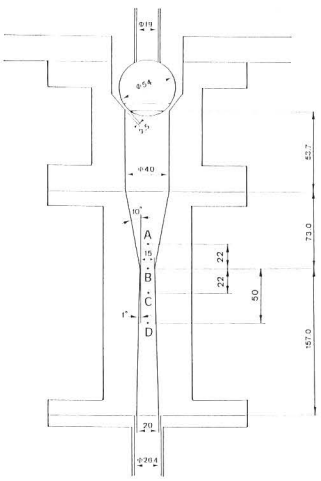

Fig. 2 Detail of test section.

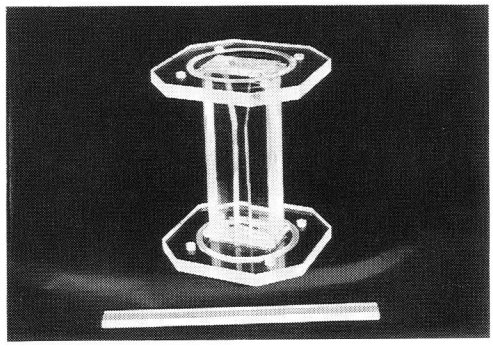

Fig. 3 Photograph of test section.

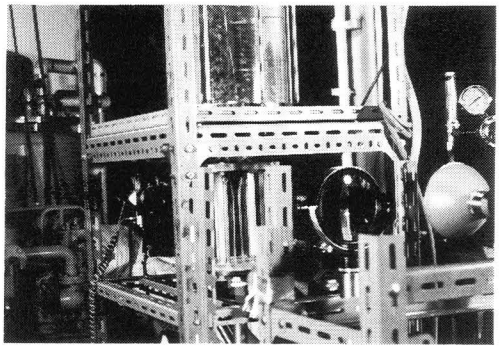

Fig. 4 Optical setup.

blowdown is several seconds. It has to be stressed that the flow realized in this facility under these conditions is always a subsonic-like flow.

The surface of the water was always set at 642.5 mm above the nozzle throat at the beginning of each run. All experiments were performed when the surface of the water in the upstream tank passed through the location at 442.5 mm above the throat after opening the shutter valve. It took at least a few seconds for the surface of the water to arrive at that location. This time was enough to get a steady bubbly flow in the present facility. The flow rate of the liquid was determined by measuring the time required for the water surface to pass through the interval of 100 mm from 542.5 mm to 442.5 mm measured from the nozzle throat.

For the visualization of bubbles, two stroboscopic light sources with a flash duration of about 1.8 μ sec were used to take double-exposure photographs. The time interval of two successive flashes was regulated arbitrarily by a digital retarder. The optical setup is shown in Fig. 4.

The pressures were measured by four sets of a TOYODA PMS-5 semiconductor pressure transducer and a TOYODA AA-6010 amplifier. These four transducers were mounted along the nozzle wall ; 22 mm upstream of the throat, at the throat, 22 mm and 50 mm downstream of the throat. All the outputs were recorded and analyzed by an NEC PC-9801 RA2 personal computer. The pressure for the steady flow was obtained by averaging the data over 1.0 sec. The sampling time of pressure fluctuations was 0.1 sec. The power spectrum density was obtained by FFT transformation of the measured data.

2-2. Bubble shape and flow pattern

It is very important to know the change in bubble shapes along the nozzle and also the flow pattern of the bubbles, because this information is helpful to understand the mechanism for the velocity slip between the liquid and the bubbles. A few photographs of the bubbles

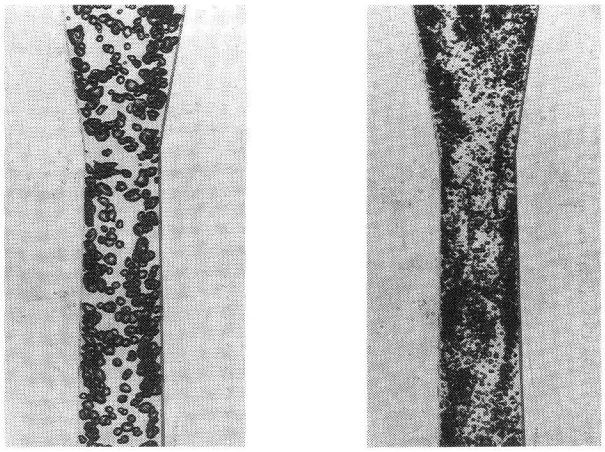

a) $\bar{p}_D = 1.013 \times 10^5$ Pa, $\dot{\bar{m}}_g = 3$ N*l*/min

b) $\bar{p}_D = 0.213 \times 10^5$ Pa, $\dot{\bar{m}}_g = 3$ N*l*/min

Fig. 5 Instantaneous photographs of bubbles for $\bar{p}_0 = 1.013 \times 10^5$ Pa.

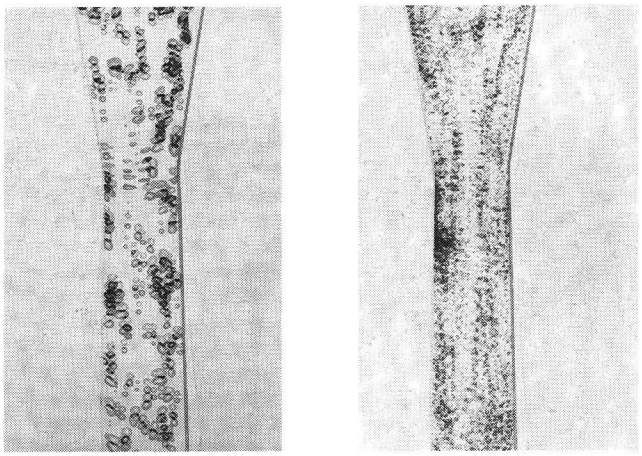

a) $\bar{p}_D = 1.013 \times 10^5$ Pa, $\dot{\bar{m}}_g = 1$ N*l*/min, $\Delta\bar{t} = 700\,\mu$ sec

b) $\bar{p}_D = 0.213 \times 10^5$ Pa, $\dot{\bar{m}}_g = 1$ N*l*/min, $\Delta\bar{t} = 300\,\mu$ sec

Fig. 6 Double-exposure photographs of bubbles for $\bar{p}_0 = 1.013 \times 10^5$ Pa.

in the nozzle are shown in Fig. 5. The bubbles in Fig. 5 are those for the gas flow rates of 1.0, 3.0 and 5.0 N*l*/min for $\Delta\bar{p} = \bar{p}_0 - \bar{p}_D = 0$, where $\bar{p}_0 (\equiv 1.013 \times 10^5$ Pa) and $\bar{p}_D$ are the pressures at the upstream tank and the downstream tank, respectively. In these cases, the mixture is blown down only due to the effect of gravitational force. In Fig. 6, $\Delta\bar{p}$ is set to

0.8×10^5 Pa ($\bar{p}_D=0.213\times10^5$ Pa).

From these, we can see that the size of the bubbles produced by the gas injector strongly depends on the pressure difference Δp and their sizes are mostly determined by the flow conditions near the gas injector. In the present experiment, the size of the bubbles produced becomes smaller with the increasing pressure difference. The observed bobble radii are about 1~3 mm for $\bar{p}_D=1.013\times10^5$ Pa and 0.1~1 mm for $\bar{p}_D<0.8\times10^5$ Pa. The distortion of the bubble shapes depends on their sizes; smaller bubbles tend to have shapes closer to spheres but larger bubbles experience larger distortion during the flow through the nozzle due to the interactions with the liquid, nozzle wall and surrounding bubbles. This distortion becomes maximum near the nozzle throat. The shape of the bubbles is flattened along a plane perpendicular to the flow direction.

The distribution of bubbles is not always uniform in space. This trend is especially prominent in the cases in Fig. 5. A phenomenon of aligned flowing of bubbles is well seen in these pictures.

Morioka et al. have suggested that the large velocity slip may be expected to occur when the bubble shapes are severely distorted due to the large pressure gradient, and also the prominent aligned-flowing of bubbles occurs in the nozzle. These are considered to be helpful for reducing the virtual inertia of the bubbles[5]. In the present experiment, abnormally large velocity slip as in their experiments has not been observed. This might come from the fact that the pressure gradient and the void fraction of the gas in the present experiment are much smaller than those in their case.

2-3. Velocity and pressure fields

The bubble velocities are measured on photographs which are taken by exposing twice at some time interval with stroboscopic light sources. The time intervals $\Delta\bar{t}$ are 700 μ sec and 300 μ sec for the cases of $\Delta\bar{p}=0$ and 0.8×10^5 Pa, respectively. Samples of these photographs are shown in Fig. 6. By measuring the distance $\Delta\bar{l}$ between the corresponding images of a bubble, local velocity of the bubble $\bar{u}_g$can be determined by $\bar{u}_g=\Delta\bar{l}/\Delta\bar{t}$.

The liquid velocity u and the void fraction of the gas α are obtained by measuring pressures of the mixture along the nozzle axis. Applying a quasi-one dimensional approximation, the liquid velocity u and the void fraction α are given by

$$\alpha=\frac{\bar{\dot{m}}_g\bar{R}\,\bar{T}}{\bar{p}\bar{u}_g\bar{A}} \tag{1}$$

$$\bar{u}=\frac{\bar{\dot{m}}}{(1-\alpha)\bar{A}} \tag{2}$$

respectively, under the assumptions,

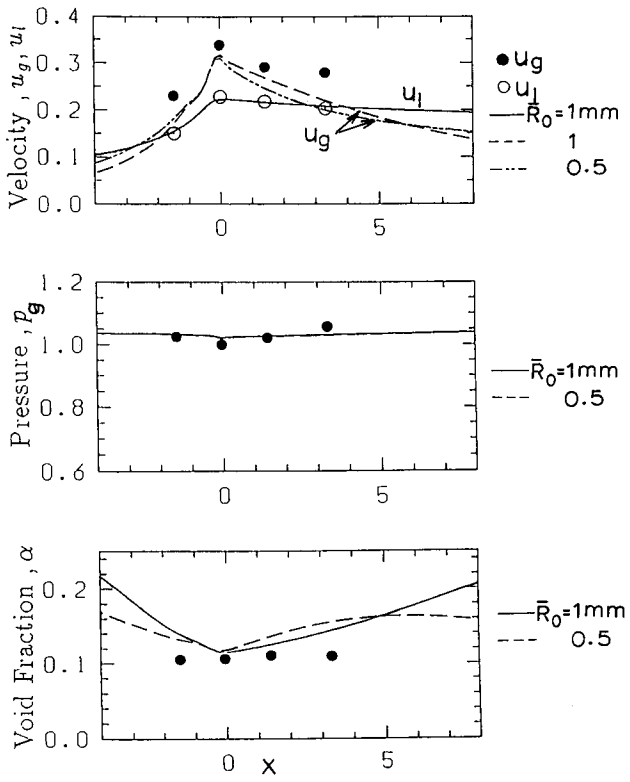

Fig. 7 Distributions of gas and liquid velocities, gas pressure and void fraction for $\bar{p}_D=1.013\times10^5$ Pa and $\bar{\dot{m}}_g=5$ Nl/min.

$$\bar{p}=\bar{p}_g(=\bar{p}_l) \tag{3}$$

$$\bar{p}_g=\bar{\rho}_g\bar{R}\,\bar{T}_g \tag{4}$$

$$\bar{T}_l=\bar{T}_g\equiv\text{const} \tag{5}$$

where R is the gas constant, T the temperature, $\bar{\dot{m}}$ the volume flow rate of liquid, $\bar{\dot{m}}_g$ the volume flow rate of gas and $\bar{A}$ the cross-sectional area of nozzle. The subscripts l and g denote the liquid and the gas, respectively. The measured pressures, velocities and void fraction are shown in Figs. 7 to 9. Since every flow is a subsonic-like flow, the bubble and liquid velocities and velocity slip are largest at the nozzle throat in every case. In the case of Fig. 9, these are about 9 m/sec, 7 m/sec and 2 m/sec, respectively, at the throat.

The relationship between the mass flow rate of the gas $\bar{\dot{m}}_g$ and the void fraction α at the throat is shown in Fig. 10. This figure shows that the void fraction in the present experiment is at most 0.1 and depends almost linearly on the mass flow rate $\bar{\dot{m}}_g$.

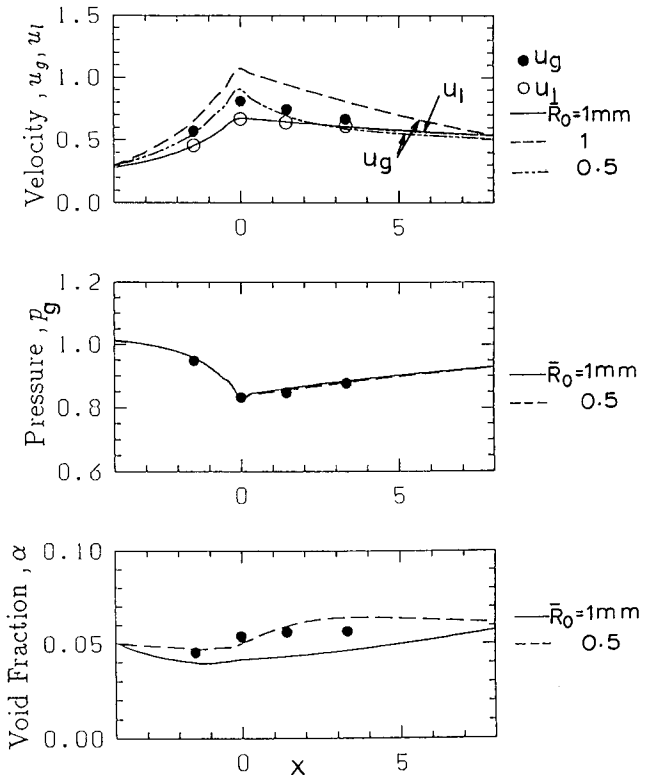

Fig. 8 Distributions of gas and liquid velocities, gas pressure and void fraction for $\bar{p}_D=0.480\times10^5$ Pa and $\bar{\dot{m}}_g=5$ Nl/min.

2-4. Pressure fluctuation

Measured power spectrum densities of the pressure fluctuation are shown in Figs. 11 to 14. The data in Figs. 11 and 12 are for $\bar{p}_D=1.013\times10^5$ Pa ($\Delta\bar{p}=0$ Pa) and those in Figs. 13 and 14 are for $\bar{p}_D=0.213\times10^5$ Pa ($\Delta\bar{p}=0.8\times10^5$ Pa). Figs. 11 and 13 suggest that the liquid flow ($\bar{\dot{m}}_g=0$) for $\Delta\bar{p}=0$ Pa is laminar but the flow for $\Delta\bar{p}=0.8\times10^5$ Pa is turbulent. Since the pressure waves propagate with the sound velocity of water (~1480 m/sec) in a pure liquid ($\bar{\dot{m}}_g=0$), the spectrum densities measured at locations $\bar{x}=-22$ mm, 0 mm, 22 mm and 50 mm should have nearly the same features. This is well seen in Fig. 13. The difference of magnitude of spectrum peaks among the data will come from the changes of local flow velocity and the cross-sectional area of the nozzle at the measured points. As shown in Fig. 10, the maximum void fraction is at most 0.1. Under this condition, the effect of presence of the bubbles does not appreciably affect the liquid velocity and pressure of mixture $\bar{p}$.

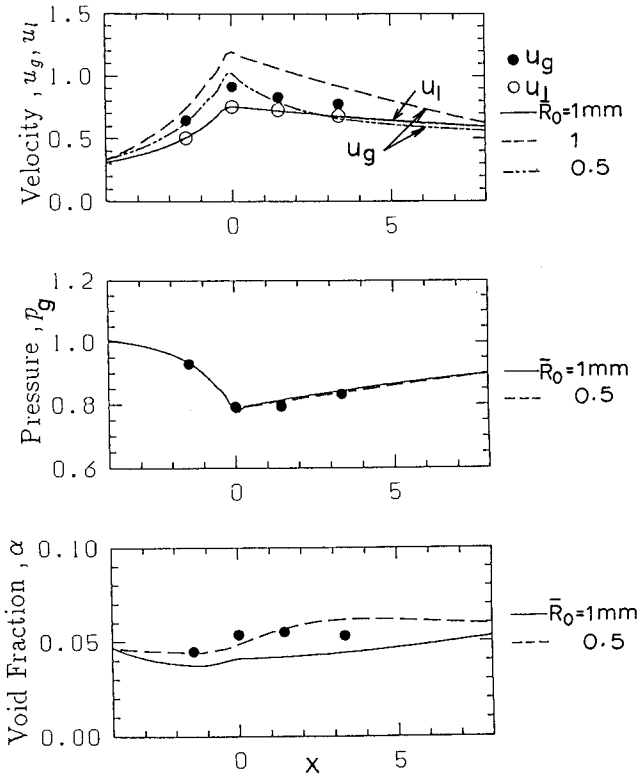

Fig. 9 Distributions of gas and liquid velocities, gas pressure and void fraction for $\bar{p}_D=0.213 \times 10^5$ Pa and $\bar{m}_g=5$ N*l*/min.

It is interesting that the bubbles generate pressure fluctuations in a frequency range as shown in Fig. 12. The frequencies of the fluctuations produced will depend mainly on the velocity slip and the sizes of bubbles included in the flow.[5] In the flow in Fig. 12, the pressure fluctuations generated by the bubbles are relatively weak and the frequency range of the fluctuations is less than about 700 Hz. Both the intensification of the fluctuations near the nozzle throat and the reduction of them downstream of the nozzle throat are not prominent in this case. When the velocity slip becomes large (Fig. 14), the presence of bubbles significantly affects the pressure fluctuations. By comparing Figs. 13 and 14., it can be seen that bubbles absorb pressure waves in some frequency range and also generate pressure fluctuations in a particular frequency range which will depend on the velocity slip and the sizes of the bubbles. The pressure fluctuations shown in Fig. 13 ($\bar{m}_g=0$) are effectively suppressed in the corresponding data in Fig. 14 ($\bar{m}_g=5$ N*l*/min), which may suggest an effective role of bubbles as absorbers of pressure fluctuations. It is, however,

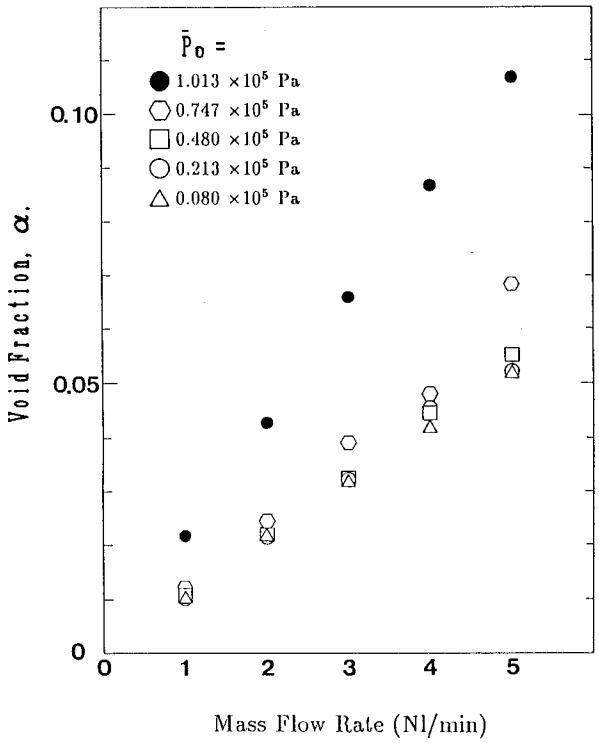

Fig. 10 Void fraction versus mass flow rate of gas for $\bar{p}_0 = 1.013 \times 10^5$ Pa.

important to point out that the bubbles also produce pressure fluctuations as in Fig. 14. These fluctuations produced are strongest near the nozzle throat and the higher part of them (>500 Hz) are effectively reduced in the downstream region of the throat.

In Ref. 5, Morioka et al. predict that intensification of pressure fluctuations in some range of frequency is caused near the nozzle throat by the velocity slip instability. On the other hand, reduction of the high frequency part of these fluctuations is caused by the cutoff of propagation waves in the region downstream of the throat. The fluctuation characteristics observed in the present experiment agree will with their prediction.

3. Numerical analysis

3–1. Governing equations

In order to explain the experimental results physically, numerical simulations were carried out using Wijngaarden's model equations. In 1967 Wijngaarden derived model equations for a dilute bubbly flow through simple averaging of the equations on the microlevel[7].

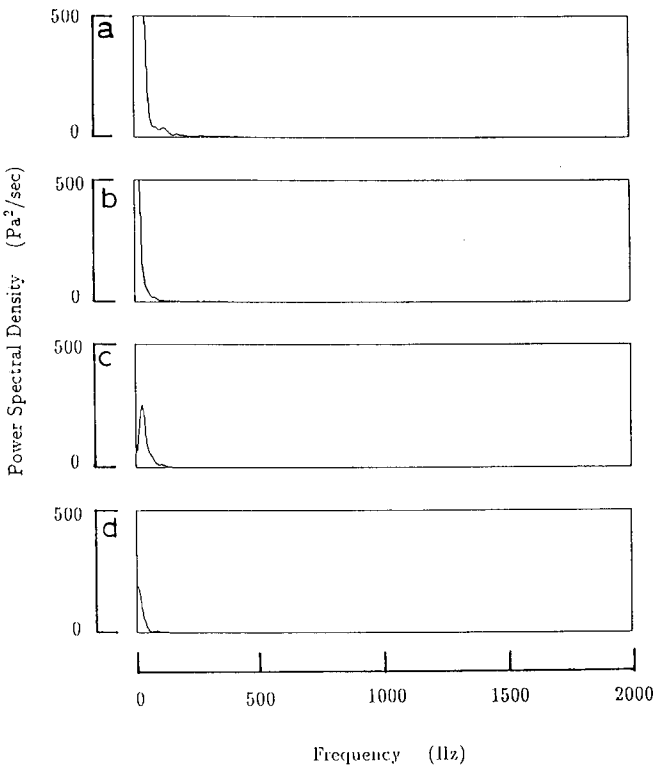

Fig. 11 Power spectrum density function of the fluctuation at four measuring points along nozzle axis for $\bar{p}_D = 1.013 \times 10^5$ Pa and $\bar{\dot{m}}_g = 0$ Nl/min.
A. $\bar{x} = -22$mm, B. $\bar{x} = 0$mm, C. $\bar{x} = 22$mm, D. $\bar{x} = 50$mm.

(Here we call these model equations old ones). The derivation of this model is somewhat intuitional but it is easy to understand its physical meaning. Later, however, it was pointed out that the system of the old model equations is not well posed as an initial value problem. Then, in 1984 Wijngaarden rederived modified model equations through a more systematic averaging technique[8]. (We call this model the new one). The derivation of the new model equations is theoretically more rigorous than that of the old ones, but this new model's physical meaning is more difficult to understand. The new model equations at least apparently constitute a complete hyperbolic system, unlike the old model equations with complex characteristics found previously.

In the present study, we used two, old and new, model equations of Wijngaarden. The flows are assumed to be quasi-one-dimensional. Important assumptions included in Wijngaarden's model equations are :

i) The mixture is composed of liquid and dispersed gas bubbles.

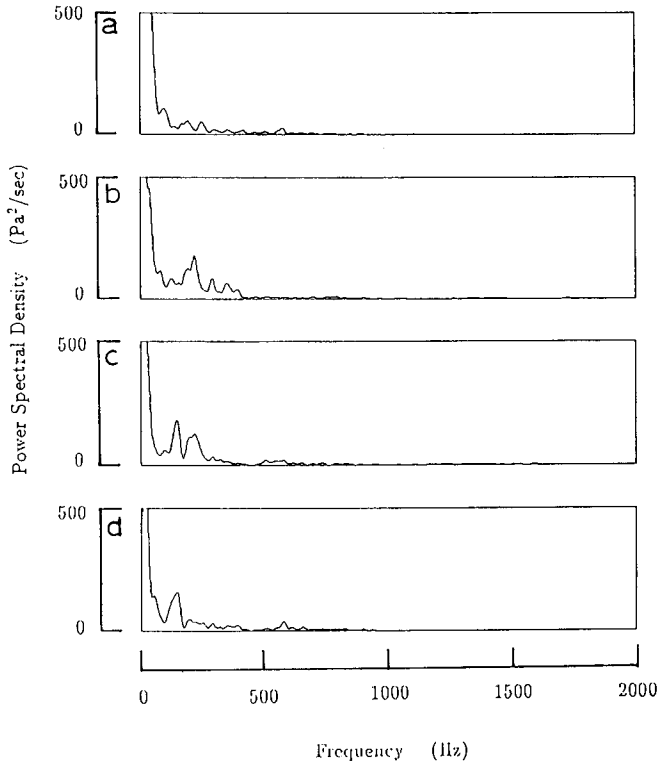

Fig. 12 Power spectrum density function of the fluctuation at four measuring points along nozzle axis for $\bar{p}_D = 1.013 \times 10^5$ Pa and $\bar{\dot{m}}_g = 5$ N*l*/min.
A. $\bar{x} = -22$mm, B. $\bar{x} = 0$mm, C. $\bar{x} = 22$mm, D. $\bar{x} = 50$mm.

ii) No phase change takes place.

iii) The liquid is incompressible and inviscid except for its interactions with the bubbles.

iv) The gas is compressible and then the bubbles can change their volume.

v) The bubbles are spheres with a locally uniform diameter and their spatial distribution is locally uniform.

vi) The suspension is so dilute that the direct interactions between bubbles are negligible.

vii) Coalescence and/or breakup of bubbles do not occur.

Before describing the model equations, nondimensional quantities are introduced by

$$\frac{\bar{t}}{\bar{L}_t/\bar{U}_r} = t, \quad \frac{\bar{x}}{\bar{L}_t} = x, \quad \frac{\bar{A}}{\bar{A}_t} = A, \quad \frac{\bar{u}}{\bar{U}_r} = u, \quad \frac{\bar{u}_g}{\bar{U}_r} = u_g,$$

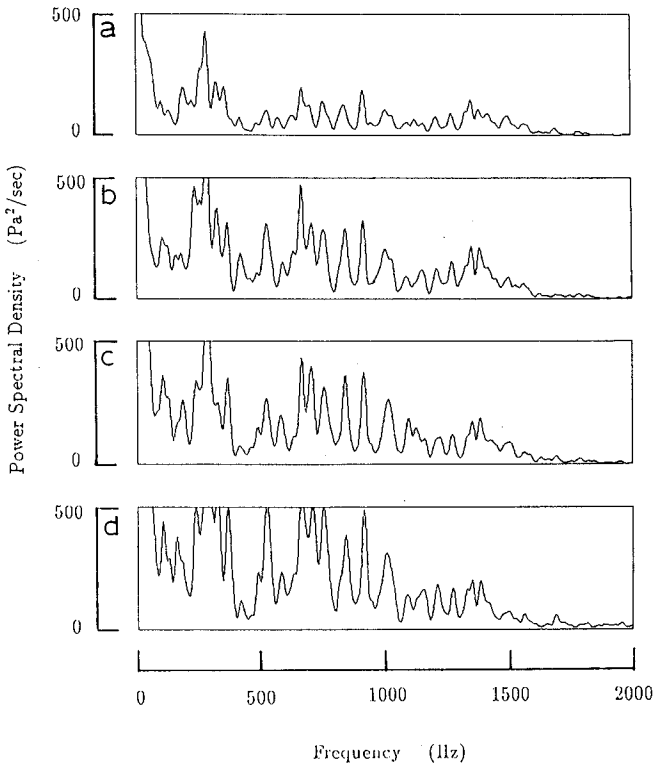

Fig. 13 Power spectrum density function of the fluctuation at four measuring points along nozzle axis for $\bar{p}_D=0.213\times10^5$ Pa and $\bar{m}_g=0$ Nl/min.
A. $\bar{x}=-22$mm, B. $\bar{x}=0$mm, C. $\bar{x}=22$mm, D. $\bar{x}=50$mm.

$$\frac{\bar{p}}{\bar{\rho}\bar{U}_r^2}=p,\quad \frac{\bar{p}_g}{\bar{\rho}\bar{U}_r^2}=p_g,\quad \frac{\bar{\rho}_g}{\bar{\rho}_{gr}}=\rho,\quad \frac{\bar{R}}{\bar{R}_r}=R, \tag{6}$$

where t is the time, x the distance along the nozzle axis, A the cross-sectional area of the nozzle, u the velocity of the liquid, ρ the density of the liquid, p the pressure of the miuture, μ the viscosity of the liquid, u_g the gas velocity, ρ_g the gas density, p_g the gas pressure, α the void fraction of the gas, R the radius of a gas bubble, L_t the throat length, A_t the cross-sectional area of the nozzle at the throat and g the acceleration of gravity. The overbars and the subscript r denote dimensional quantities and reference conditions, respectively. The direction of the gravitational force is taken to be along the nozzle axis.

Furthermore, for later convenience, nondimensional parameters are defined by

$$k=\frac{\bar{R}_r}{\bar{L}_t},\quad Re=\frac{\bar{\rho}\bar{U}_r\bar{L}_t}{\bar{\mu}},\quad \gamma=\frac{\bar{p}_{gr}}{\bar{\rho}\bar{U}_r^2},\quad \Gamma=\frac{\bar{U}_r^2}{g\bar{L}_t} \tag{7}$$

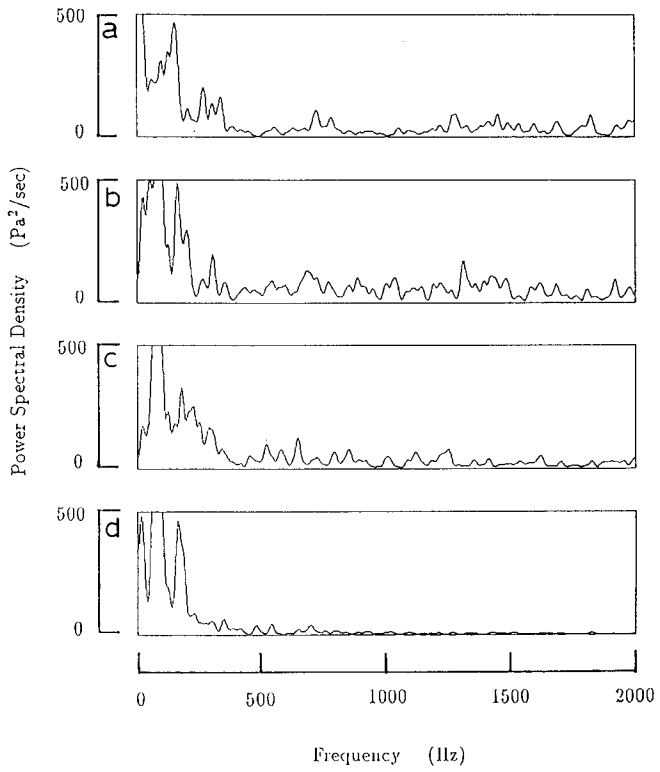

Fig. 14 Power spectrum density function of the fluctuation at four measuring points along nozzle axis for $\bar{p}_D=0.213\times10^5$ Pa and $\bar{\dot{m}}_g=5$ Nl/min.
A. x=−22mm, B. x=0mm, C. x=22mm, D. $\bar{x}$=50mm.

where Re and Γ are the Reynolds and Froude numbers, respectively.

In the present analysis, reference quantities are specified as follows :

$$\bar{\rho}=1.0\times10^3\ \text{kg/m}^3,\quad \bar{\rho}_{g0}=1.25\ \text{kg/m}^3,\quad \bar{U}_r=10\ \text{m/s},\quad \bar{R}_r=1.0\times10^{-3}\ \text{m},$$
$$\bar{L}_t=1.5\times10^{-2}\ \text{m},\quad \bar{A}_t=\bar{L}_t\bar{D}=1.5\times1.5\times10^{-4}\ \text{m}^2,\quad \bar{\mu}=1.002\times10^{-3}\ \text{kg/m.s}$$
$$\bar{g}=9.8\ \text{m/s}^2, \tag{8}$$

which yield

$$k=0.08,\quad Re=1.5\times10^5,\quad \gamma=0.81,\quad \Gamma=8.85\times10^2 \tag{9}$$

With the nondimensional quantities defined above, the governing equations of the system following Wijngaaden's old model can be written in the from :

$$\frac{\partial}{\partial t}(1-\alpha)A+\frac{\partial}{\partial x}(1-\alpha)uA=0, \tag{10}$$

$$\frac{\partial}{\partial t}(\alpha\rho_g A)+\frac{\partial}{\partial x}(\alpha\rho_g u_g A)=0 \tag{11}$$

$$\frac{\partial}{\partial t}[(1-\alpha)uA]+\frac{\partial}{\partial x}[(1-\alpha)u^2A]=-A\frac{\partial p}{\partial x}+\frac{1}{\Gamma}(1-\alpha)A \tag{12}$$

$$\frac{\partial}{\partial t}[\alpha(u_g-u)A]+\frac{\partial}{\partial x}[\alpha u_g(u_g-u)A]=-2\alpha A\frac{\partial p}{\partial x}-\frac{18}{R_e k^2}\alpha\rho_g AR(u_g-u) \tag{13}$$

$$p_g-p=k^2\left[R\frac{d^2R}{dt^2}+\frac{3}{2}\left(\frac{dR}{dt}\right)^2\right]+\frac{4}{Re}\frac{1}{R}\frac{dR}{dt} \tag{14}$$

$$\rho_g R^3=1, \tag{15}$$

$$\frac{p_g}{\rho_g}=\gamma \tag{16}$$

where

$$\frac{d}{dt}=\frac{\partial}{\partial t}+u_g\frac{\partial}{\partial x} \tag{17}$$

Here it is assumed that the flow is isothermal and the effect of surface tension on the volume change of a bubble is neglected.

Following Wijngaarden's new model, Eq. (13) is replaced by

$$\frac{d}{dt}[R^3(u_g-u_0)]=2R^3\frac{du_0}{dt}-\frac{18R}{Rek^2}(u_g-u_0)-\frac{2}{\Gamma}R^3 \tag{18}$$

where

$$u_0=(1-\alpha)u+\alpha u_g \tag{19}$$

3-2. Steady solution

The numerical scheme employed here is a time-dependent two-step MacCormack one. First, Eqs. (10) to (12), (15) and (16) are solved analytically under simplifying assumptions, $u_g=u$ and $p_g=p$. The flow model given by using $u_g=u$ is called the miutxre model and that given by using $p_g=p$ is called the one-pressure model. The flow conditions obtained above are used as initial flow conditions to get a time-converged or a steady solution for Eqs. (10) to (16) by the time-dependent method. The computational domain is shown in Fig. 15.

Samples of steady solutions for supersonic-like and subsonic-like flows are shown in Fig. 16. As in the nozzle flows of a compressible gas, the choking phenomena occurs when

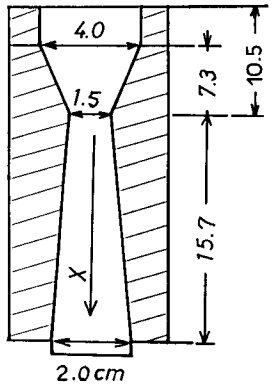

Fig. 15 Computational domain.

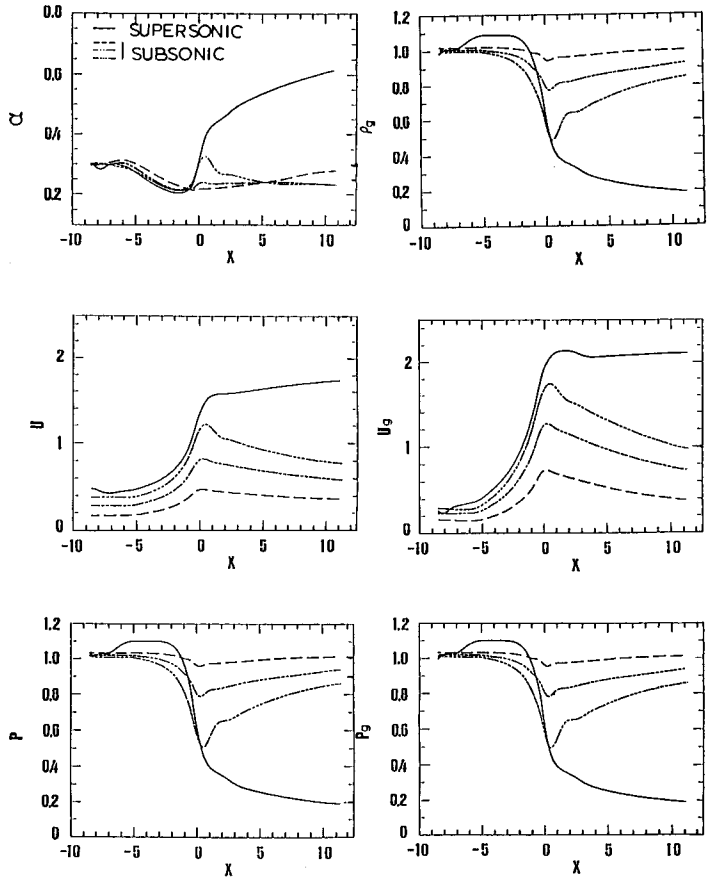

Fig. 16 Subsonic like and supersonic like solutions for $\bar{p}_0 = 1.013 \times 10^5$ Pa and $\alpha_0 = 0.3$.

the exit pressure becomes lower than some critical value for fixed conditions at the upstream tank. Each numerical solution was obtained for a specified reservoir pressure p_0, exit pressure p_D, mass flow rates of gas and liquid and bubble radius R_0 at the upstream tank, where the subscript zero denotes conditions at the upstream tank.

Obviously, the gas velocity u_g deviates appreciably from the liquid velocity u. The mixture pressure p is, however, very close to the gas pressure p_g in the whole flow region both in the supersonic–like and subsonic–like solutions. This means the mixture model will not be suited for the analysis of nozzle flow, but the one–pressure approximation will be useful for the analysis. In the present experiment, we used the one–pressure approximation to determine the local liquid velocity and void fraction with the measured pressure p. The unmerical solutions support such a treatment.

Numerical results for the subsonic like flows are shown in Figs. 7–9 and 17 for the same conditions as the experimental ones. Since in the experiment it is difficult to determine the bubble radius, the numerical results are obtained for two different bubble radii at the upstream tank. In Fig. 17, effects of the bubble radius at the upstream tank on the flow quantities in the nozzle are shown for fixed pressure conditions at the upstream tank and nozzle exit and a fixed mass flow rate of gas. It has to be stressed that the bubble radius

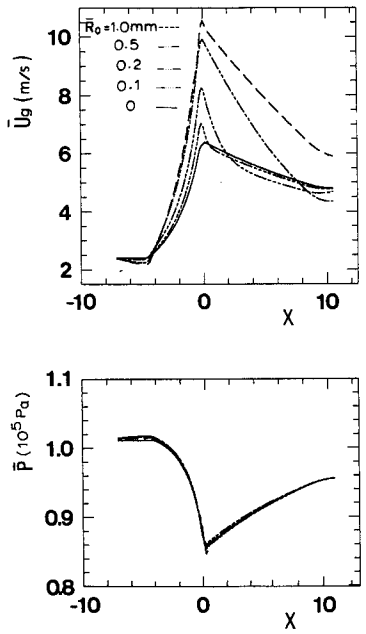

Fig. 17 Distributions of bubble velocity and pressure of mixture for various bubble radius $\bar{R}_0$ at upstream tank for $\bar{p}_0=1.013\times10^5$ Pa, $\bar{p}_D=0.480\times10^5$ Pa and $\bar{\dot{m}}_g=3$ Nl/min.

affects the bubble velocity but does not affect the pressure of the mixture and then the liquid velocity. This is quite reasonable because the void fraction considered here is at most 0.1 and so very small.

As shown in Figs. 7 to 9, agreement between the numerical and experimental results is very good, especially for the pressure and liquid velocity distributions. As for the bubbly velocity and void fraction, they are somewhat different from each other. This will come from the deformation of the bubble shape from a sphere in the region near the nozzle throat.

3–3. Propagation of pressure fluctuation

For investigation of flow instability, unsteady behaviors of the bubbly flow in the nozzle are simulated numerically. The steady solution obtained in the previous section is used as an

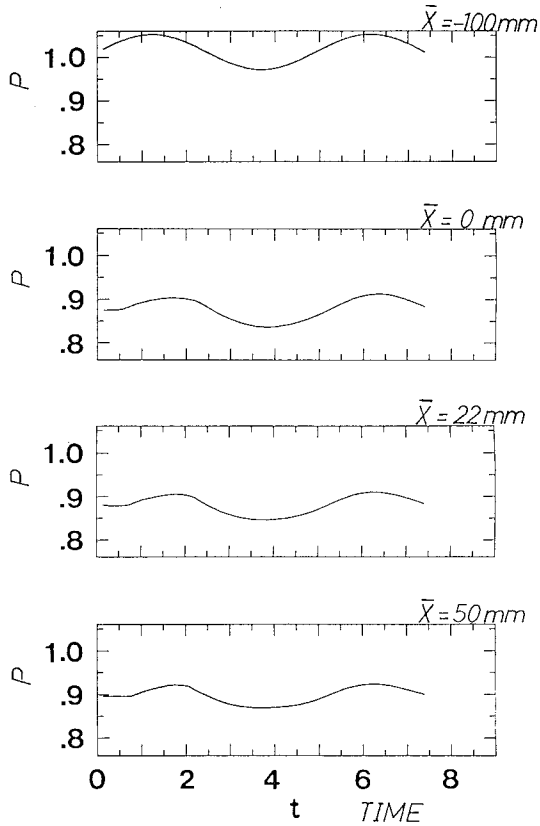

Fig. 18 Propagation of pressure waves for $\bar{p}_0 = 1.013 \times 10^5$ Pa, $\bar{p}_D = 0.747 \times 10^5$ Pa, $\bar{\dot{m}}_g = 3$ Nl /min and $\bar{f} = 400$Hz.

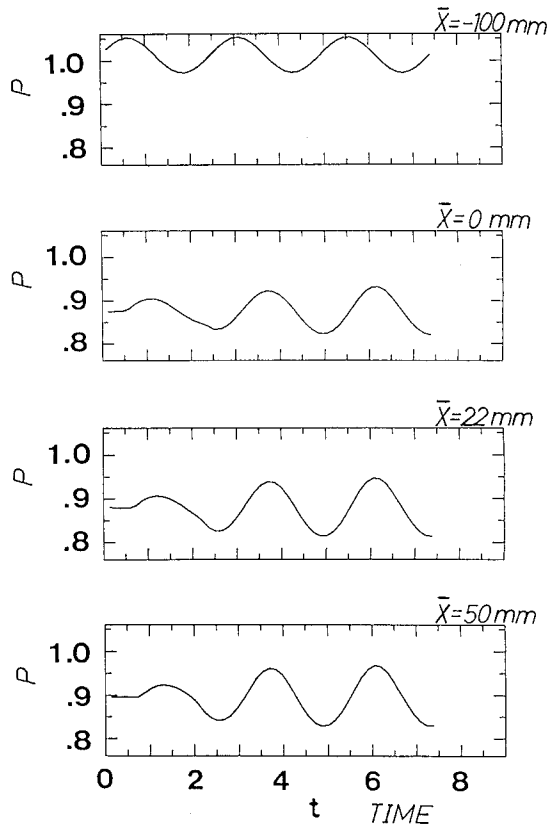

Fig. 19 Propagation of pressure waves for $\bar{p}_0=1.013\times10^5$ Pa, $\bar{p}_D=0.747\times10^5$ Pa, $\bar{m}_g=3$ N*l*/min and $\bar{f}=800$Hz.

initial flow for the unsteady calculation. A pressure fluctuation Δp

$$\Delta p=0.04\sin(2\pi\bar{f}\bar{t}) \tag{20}$$

is imposed on the pressure at the upstream boundary, which is the pressure of the steady solution, and $\bar{f}$ is the frequency of the pressure disturbance. After initiation of the unsteady calculation, the pressure fluctuation continues to be imposed at the upstream boundary and the change of pressure fluctuation with time in the nozzle is obtained numerically.

Propagation of the pressure disturbance is shown in Figs. 18–20 for $\bar{f}=400$ 800 and 1600 Hz. For $\bar{f}=400$ Hz, the amplitude of the pressure disturbance does not change along the nozzle axis, but for $\bar{f}=800$ Hz, it grows larger with the increasing nozzle distance. On the other hand, for $\bar{f}=1600$ Hz, it decays in the downstream region of the throat, which means that the wave is cut off. These features will, at least qualitatively, agree well with the present experiment and also with the theoretical predictions by Morioka et al.

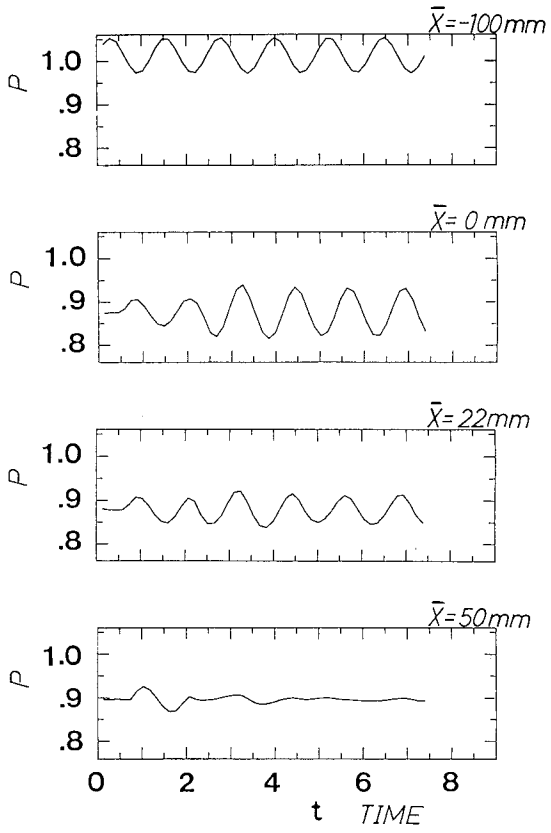

Fig. 20 Propagation of pressure waves for $\bar{p}_0=1.013\times10^5$ Pa, $\bar{p}_D=0.747\times10^5$ Pa, $\bar{m}_g=3$ N*l*/min and $\bar{f}=1600$Hz.

The numerical results discussed previously were those obtained by using Wijngaaden's old model equations. It is interesting to investigate differences between solutions obtained using Wijngaaden's old and new model equations. For this purpose, similar numerical simulations have been carried out using the latter model equations. Unfortunately, however, no steady solution could be obtained. For all flow conditions considered here, the system of his new model equations was always numerically unstable and the solution broke up near the nozzle throat. Fig. 21 demonstrates the numerical instability of the time-dependent solution, where the approximate solution given by putting $u_g=u$ and $p_g=p$ was used as initial flow conditions as in the previous case and n is the integration time step. It has to be stressed that this does not always mean that his new model is wrong. It is quite possible that the bubbly flow is essentially unstable when the velocity slip appears in the flow and the new model equations might reflect this fact. To get a decisive conclusion about the physical reasonableness of his new model, more systematic and careful numerical simulations will be

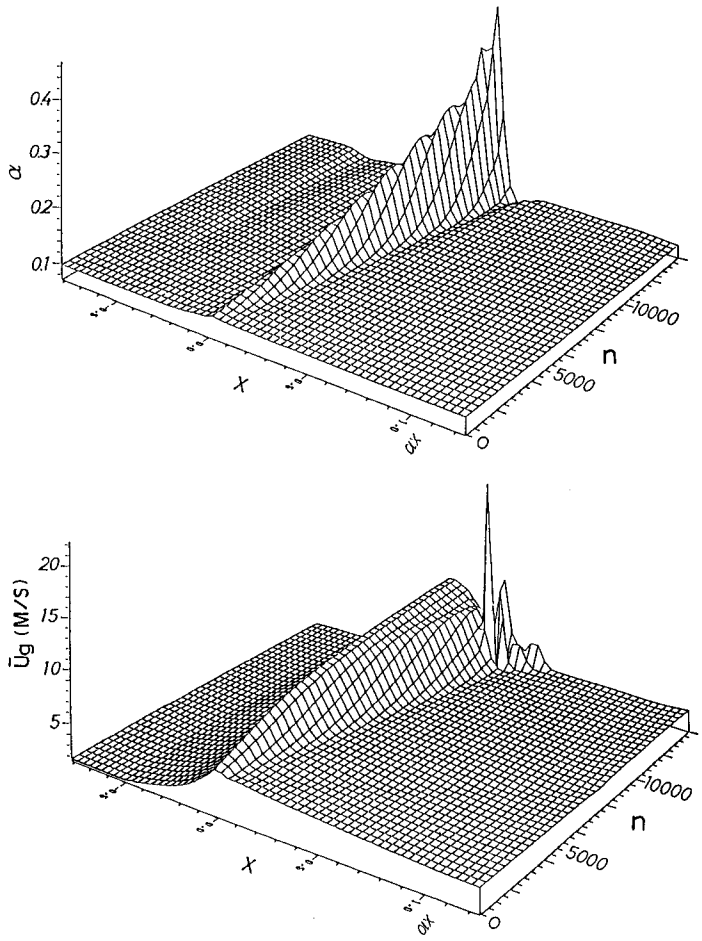

Fig. 21 Numerical instability of a time–dependent solution for Wijngaarden's new model equations.

needed.

4. Conclusions

Flow characteristics of a mixture composed of liquid and dispersed gas bubbles are investigated experimentally and numerically.

Time–averaged or steady distributions of velocities, pressures of liquid and gas, and void fraction along the nozzle axis were obtained experimentally. It was confirmed that these experimental results agree well with the numerical simulations using Wijngaarden's old

model equations.

As in Ref. 5, it was demonstrated that the intensification of pressure fluctuations and their cutoff occur in the nozzle. These phenomena strongly depend on the velocity slip and the void fraction. At least for the present it is not clear what the energy of pressure fluctuations convert to when they decay by cutoff phenomena.

Numerical simulations using the Wijngaaden's new model equations did not give any steady state solution and always broke up near the nozzle throat for all flow conditions considered here. Mathematically it is confirmed that the system of equations has a critical point at $\alpha = 1/3$. Numerical instability, however, occurred in all cases without respect to the magnitude of the void fraction.

Acknowledgements

The authors would like to acknowledge support through grant-in-aid for Scientific Research (C-03805007) of the Ministry of Education, Science and Culture in Japan.

Biblioqraphy

1) J. F. Muir and R. Eichorn. "Compressible Flow of an Air-Water Mixture through a Vertical, Two-Dimensional, Converging-Divergln Nozzle". Proc. of the Heat transfer and Fluid Mechanics Institute (Stanford Univ.) pp. 183-204, 1963.

2) T. Toma, K. Yoshino and S. Morioka. "Mechanism of Velocity Slip and Associated Turbulence in Accelerating Nozzle Flow of Bubbly Liquid", Proc. 9th Conf. MHD EPG, 1986.

3) S. Morioka and T. Toma. "Stability of Two-Phase Liquid Metal MHD Channel Flows", Progress in Astronautics and Aeronautics, Vol. *100*, pp. 317-328, 1984.

4) T. Toma and S. Morioka. "Acoustical Waves Forced in Flowing Bubbly Liquid", J. Phys. Soc. Jpn, Vol. *55*, pp. 465-474, 1968.

5) T. Toma, K. Yoshino and S. Morioka. "Fluctuation characteristics of bubbly liquid flow in convergent-divergent nozzle. Fluid Dynamic Research, Vol. *2*, pp. 217-222, 1988.

6) L. Noordzij and L. van Wijngaarden. "Relaxation Effects, Caused by Relative Motion, on Shock Waves in Gas-Bubble Liquid Mixtures", J. Fluid Mech., vol. *66*, pp. 115-143, 1974.

7) L. van Wijngaarden. On the equation of motion for a mixture of liquid and gas bubbles, J. Fluid Mech., vol. *33*, pp. 465-474, 1968.

8) A. Biesheuvel and L. van Wijngaarden. Two-phase flow equations for a dilute dispersion of gas bubbles in liquid. J. Fluid Mech., vol. *148*, pp. 301-318, 1984.